



# Effect of Heat Treatment and Reinforcement Content on the Wear Behavior of Al–4Cu/Al<sub>2</sub>O<sub>3</sub>–CNT Nanocomposites

Emre Özer<sup>1</sup> · Mehmet Ayvaz<sup>2</sup> · Mustafa Übeyli<sup>3</sup> · İbrahim Sarpkaya<sup>3</sup>

Received: 16 December 2023 / Accepted: 5 February 2024  
© The Author(s) 2024

## Abstract

In the study, the effects of hybrid reinforcement (nano-alumina and MWCNT) and heat treatment on the wear behavior of the Al–4Cu nanocomposites were investigated under dry sliding condition against W–6Co ball by means of a ball-on-disk type tribometer. The load and the sliding speed were kept constant and selected to be 10 N and 0.1 m s<sup>-1</sup>, respectively, in the course of the wear tests. Meanwhile, the wear tests were completed after a total sliding distance of 1500 m was reached for each case. During these tests, the wear loss of the nanocomposites was measured at every 250 m. The worn surfaces of the nanocomposites were examined with the help of stereo and scanning electron microscopes. The volumetric wear rates, wear coefficients and wear mechanisms were identified for the nanocomposites to clarify the influence of reinforcement content and heat treatment on their wear resistance. The volume loss at the wear distance of 1500 m was obtained as 24.9 and 8.2 mm<sup>3</sup> for the annealed and aged Al–4Cu alloy, respectively. On the other hand, it decreased to 4.6 and 3.2 mm<sup>3</sup> in the case of the nanocomposites with 15% hybrid reinforcement in the annealed and aged conditions, successively. Moreover, increasing the hybrid reinforcement amount decreased the wear loss of the aged nanocomposites substantially in such a way that it resulted in the mild wear.

**Keywords** Aluminum nanocomposite · Hybrid reinforcement · Multiwall carbon nanotube · Wear · Powder metallurgy · Mechanical alloying

## 1 Introduction

Metal matrix nanocomposites (MMNs) have a great potential to achieve higher performance in automotive, defense, biomedical and aerospace applications [1]. Aluminum and magnesium come into prominence to be used as matrix material in MMNs due to their low density [1]. Aluminum nanocomposites have been proposed to be used in a wide range of applications to take the advantage of their distinguished mechanical properties compared to conventional aluminum composites and aluminum alloys in recent times

[1, 2]. Therefore, they are evaluated as an innovative material group for consideration to be used in multi-purpose applications, especially under wear conditions [1–3]. Wear of engineering materials takes place under the effects of friction caused by their interactions with other substances in relative motion, impact and corrosion [4, 5]. Wear can cause a significant loss of material from working materials with time depending on the conditions. The deterioration of precise tolerances and dimensional accuracies of working parts by wear loss can create a reduction in their mechanical performance, structural integrity and lifetime seriously [4, 5]. Therefore, wear resistance appears to be the most critical property for engineering materials operating under the threat of frictional motions, impact and corrosion in order to conserve and sustain their structural integrity, working performance and long life [4, 5]. Hence, the development, testing and utilization of new wear-resistant materials should be of primary concern under these circumstances.

In aluminum nanocomposites, the general tendency is to use nano-sized reinforcing phases to attain higher mechanical properties [1, 2]. In this type of composites, nano-ceramic

✉ Mustafa Übeyli  
mubeyli@gmail.com

<sup>1</sup> Faculty of Engineering and Natural Sciences, Industrial Engineering, Osmaniye Korkut Ata University, 80000 Osmaniye, Turkey

<sup>2</sup> Vocational School of Manisa Technical Sciences, Manisa Celal Bayar University, 45140 Manisa, Turkey

<sup>3</sup> Faculty of Engineering and Natural Sciences, Mechanical Engineering, Osmaniye Korkut Ata University, 80000 Osmaniye, Turkey



particles [2] and carbon nanotubes [1] come into prominence due to their unique properties [1, 2]. It is well known that nanoparticles and nanostructured matrix enhance the hardness and strength of the composites by obstructing the dislocation motion in a more effective way [1–3]. They also lead to improve the wear resistance of nanocomposites by achieving higher hardness and strength levels [1]. A number of studies indicated that the addition of multi-wall carbon nanotubes (MWCNTs) [6–9] or alumina particles [10–16] resulted in the higher strength levels of aluminum nanocomposites. Moreover, the incorporation of MWCNT into the aluminum matrix caused a reduction in the wear loss [17–20].

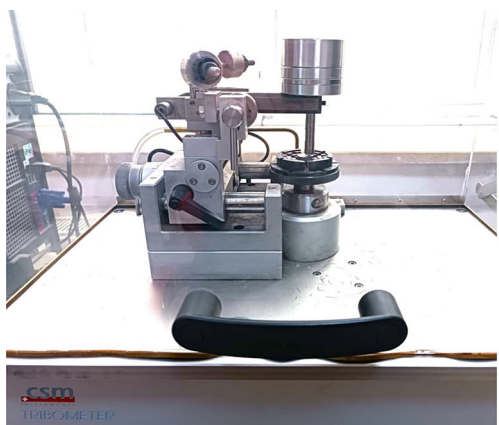
In more recent times, the use of hybrid reinforcement, consisting of MWCNT and ceramic particles, in the nanocomposites was attempted by a number of researchers [21–32]. It was reported that a more uniform dispersion of the reinforcements in the composites can be reached with this way by reducing their agglomeration throughout the matrix [21–25]. This could help to handle better microstructural features and mechanical properties [21–25]. Alizadeh et al. [26] examined the influence of hybrid reinforcing constituents, namely carbon nanotube and  $B_4C$ , on the wear and creep properties of AA5083 composites. They declared that the incorporation of boron carbide (5 or 10% in volume) to the AA5083 composite having 5 vol% CNT improved the wear resistance remarkably [26]. Zayed et al. [27] manufactured the aluminum composites reinforced with alumina or alumina + MWCNT by hot isostatic pressing [27]. It was obtained that the small amount of MWCNT addition (0.5 to 2 vol%) to  $Al_2O_3$  reinforced aluminum composites decreased the wear loss drastically. Ostovan et al. [28] characterized the tensile and wear behaviors of AA5083 surface composites that were reinforced with 5 wt% of MWCNT and  $Al_2O_3$  and manufactured by friction stir processing [28]. It was reported that the utilization MWCNT together with nano-alumina particles in the composites improved the wear resistance in comparison with the composites reinforced only with either MWCNT or  $Al_2O_3$  in equal amount [28]. The studies in regard to the wear behavior of CNT and ceramic particulate (hybrid) reinforced aluminum nanocomposites are very rare [26–28]. And also, there are no studies pertinent to the effect of thermal treatment on the wear characteristics of such nanocomposites reported. In this study, the hybrid (MWCNT and nano- $Al_2O_3$  particulates) reinforced Al–4Cu nanocomposites were fabricated with the aid of powder metallurgy technique which consisted of mechanical alloying, cold pressing and microwave sintering steps. And then, the wear behavior of these aluminum nanocomposites was investigated using the ball-on-disk method. Wear losses, wear coefficients and volumetric wear rates (VWRs) were determined for the investigated nanocomposites. In addition, the wear mechanisms of the tested nanocomposites were detected with the aid of microscopic analyses.

The main goal of the current work was to seek the effects of hybrid reinforcement amount and thermal treatment on the wear resistance of the Al–4Cu/MWCNT +  $Al_2O_3$  nanocomposites. In this context, the determination of the variations of wear rates, wear losses and wear mechanisms with respect to the reinforcement ratio and the heat treatment of these nanocomposites was targeted.

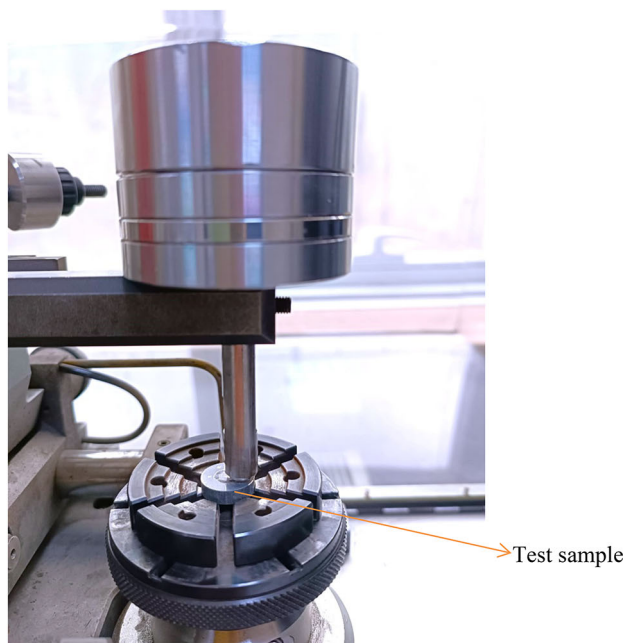
## 2 Material and Methodology

In this study, the hybrid reinforced aluminum nanocomposites were produced by cold pressing at 800 MPa and microwave sintering (at 575 °C for the unreinforced alloy and 615 °C for the nanocomposites) after the mechanical alloying of Al (144  $\mu$ m), Cu (18.3  $\mu$ m), MWCNT (1.5  $\mu$ m long and 9.5 nm diameter) and nano- $Al_2O_3$  (80 nm) powders for 5 h. The shape of Al, Cu and  $Al_2O_3$  particles was irregular and mostly rounded while that of MWCNT was in tubular form [32]. The Al–4Cu was considered as the matrix, while the CNT and  $Al_2O_3$  particles were selected to be the hybrid reinforcing phases. And then, the annealing (at 400 °C for 2 h) and artificially peak aging (at 200 °C for 11 h) treatments were applied to these materials, individually. The details of the powder morphology, manufacturing and heat treatment of these composites can be found in our previous study [32]. In the composites, the volumetric fraction of MWCNT was kept constant as 1.5%, whereas that of alumina was varied between 4.5 and 13.5% for the sake of comparison with our previous study [32], in terms of mechanical and wear characteristics. Therefore, the total reinforcement ratio in volume was considered to be 0, 6, 9, 12 and 15% for the samples; C0, C6, C9, C12 and C15, respectively. In addition, the symbols of O and T6 in the samples codes were used to differentiate annealing and aging treatments, respectively [32, 33]. The disk-shaped specimens having 20 mm diameter and 10 mm thick were set for the ball-on-disk tests.

After the heat treatment stages, the Vickers microhardness of the nanocomposites and the ball was determined using a load of 100 g in accordance with the ASTM E384-17 [34]. Meanwhile, the unlubricated sliding wear tests were done with a ball-on-disk type tribometer (CSM Instruments) in accordance with the ASTM G99-17 [35]. The tribometer used in wear testing of Al–4Cu and Al–4Cu/ $Al_2O_3$ –MWCNT nanocomposites is shown in Fig. 1. In these tests, a load of 10 N was enforced with a 6-mm-diameter WC–6Co ball. In all wear tests, the sliding speed was adjusted to be 0.1 m s<sup>−1</sup> while the total sliding distance was taken to be 1500 m. The wear loss measurements during the wear testing of samples were taken at every 250 m. Besides, all the wear tests were repeated three times for each sample type. Furthermore, the macro-pictures from the worn surfaces of the nanocomposites were taken by means of a



a)



b)

Fig. 1 Tribometer used in the wear tests: a General view, b Loading unit

stereo microscope (NIKON SMZ745T) after finishing the wear tests. Meantime, their microstructural investigations were carried out with the aid of scanning electron microscopes (FEI QUANTA FEG 250 and ZEISS SIGMA 300 VP) to reveal the wear mechanisms with respect to the reinforcement content and the heat treatment. The volumetric wear losses, the wear coefficients, the VWRs and the friction coefficients were determined for both the nanocomposites and the alloy. The specific wear rate can be calculated with Eq. 1 [5, 36]:

$$\text{Specific Wear Rate} = \frac{V}{P \cdot L} \tag{1}$$

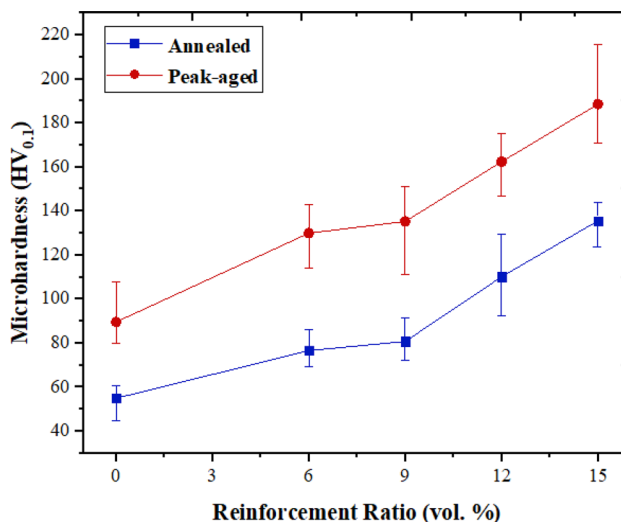


Fig. 2 The microhardness of the nanocomposites

In order to get the wear coefficient of the nanocomposites, the Archard’s equation [5, 37] is widely used and given below:

$$V = K \frac{PL}{H} \tag{2}$$

$V$  = Volume loss (mm<sup>3</sup>),  $K$  = Standard wear coefficient,  $P$  = Load (N),  $L$  = Sliding distance (mm),  $H$  = Hardness of wearing surface (kg mm<sup>-2</sup>).

However, Yang [38] mentioned that the Archard’s equation is valid under steady-state wear conditions. Therefore, the modification of the Archard’s formula was suggested to omit the transient wear part and to get more accurate and precise wear coefficient values [38]. In order to get the net steady-state wear coefficient ( $K_N$ ), the steady-state volume loss ( $V_S$ ) and sliding distance ( $L_S$ ) were introduced in the modified Archard’s equation [38]:

$$V_S = V_q - V_t \tag{3}$$

$$L_S = L_q - L_t \tag{4}$$

$V_q$  = Total volume loss (mm<sup>3</sup>),  $V_t$  = Volume loss in transient wear (mm<sup>3</sup>),  $L_q$  = Total sliding distance (mm),  $L_t$  = Sliding distance in transient wear (mm).

In this study, both the  $K$  and  $K_N$  values were computed for the investigated cases using the relations given above [5, 37, 38].

### 3 Results and Discussion

The sintered density of the C0, C6, C9, C12 and C15 was obtained to be 2.666, 2.676, 2.700, 2.698 and 2.681 g·cm<sup>-3</sup>,

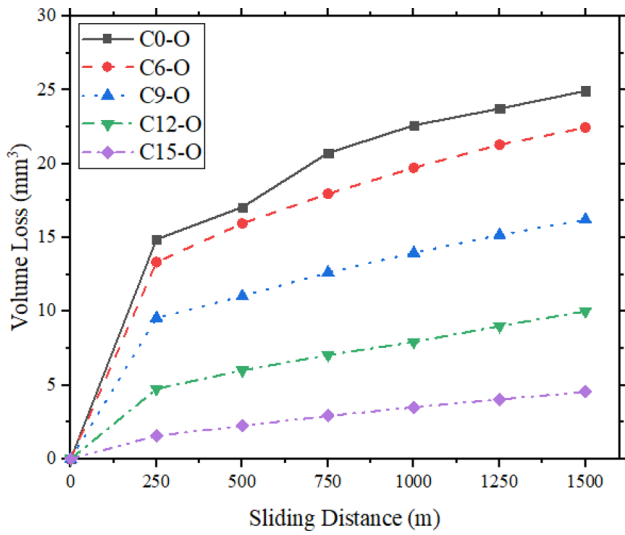


Fig. 3 Volume loss of the annealed samples

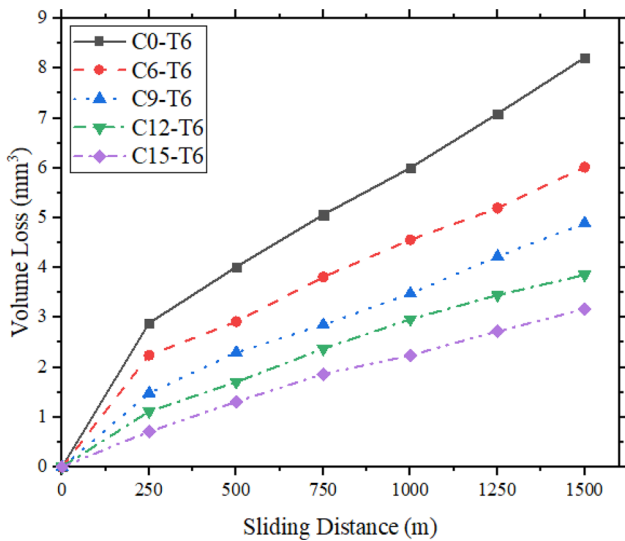


Fig. 4 Volume loss of the artificially aged samples

respectively, in our previous study [32]. Meanwhile, the porosity level of these materials was nearly 4, 5.2, 5.4, 6.6 and 8.2%, in the given order [32]. The microhardness of the specimens either annealed or artificially aged is depicted in Fig. 2. It rises with increase in the reinforcement fraction significantly and reaches ~ 136 and 189 Vickers for the annealed and peak-aged C15 sample, respectively. The aged nanocomposites have much higher hardness levels than the annealed counterparts, as expected. On the other hand, the Brinell hardness was recorded as 86.4, 119.3, 126.3, 139.8 and 163.1 for the C0-T6, C6-T6, C9-T6, C12-T6 and C15-T6, while it was

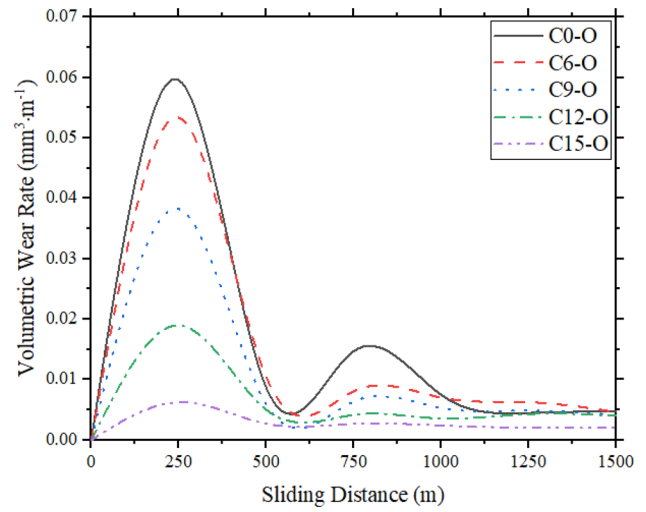


Fig. 5 Volumetric wear rate of the annealed samples

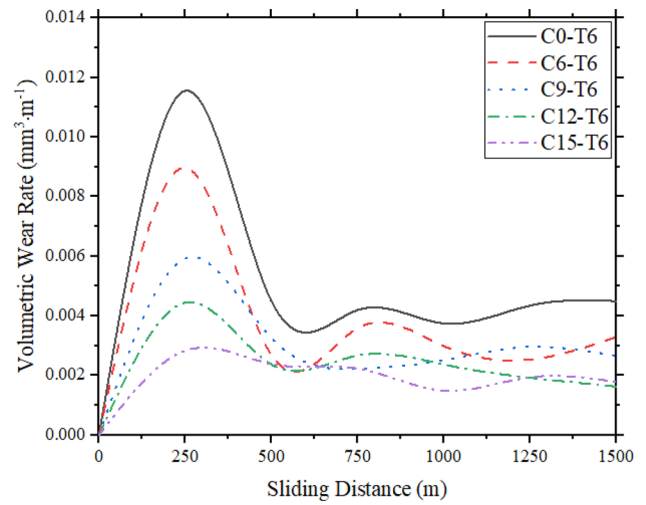


Fig. 6 Volumetric wear rate of the artificially aged samples

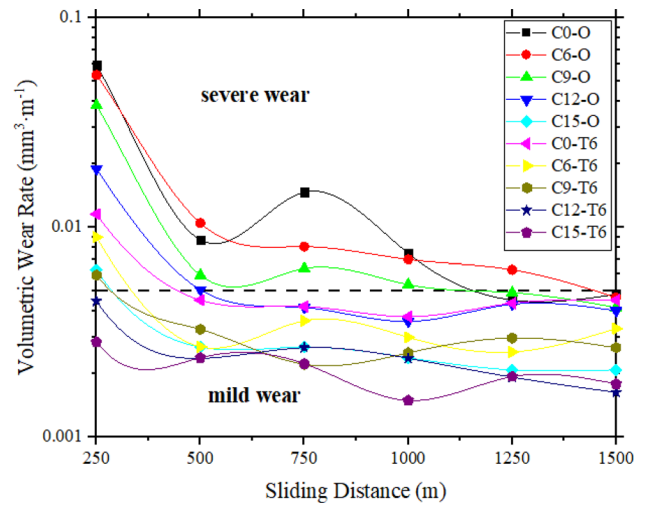


Fig. 7 Wear rate map for samples at different sliding distances

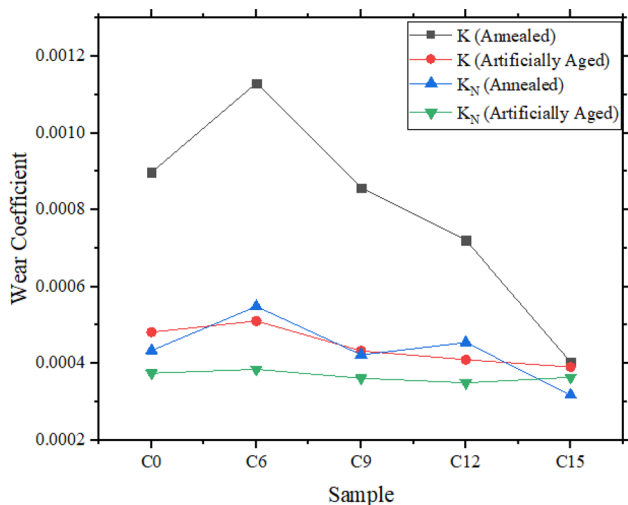


Fig. 8 Wear coefficients of the samples

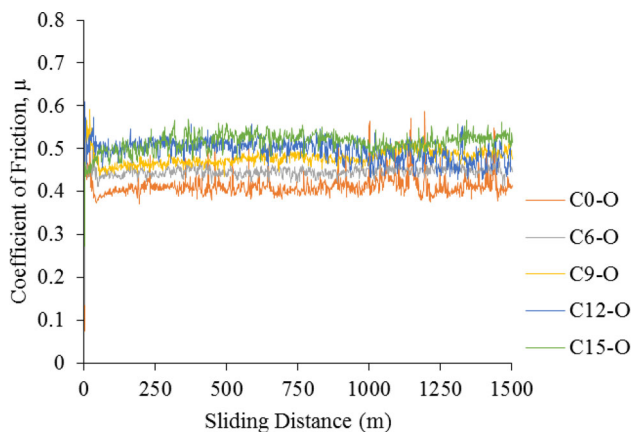


Fig. 9 Friction coefficients of the annealed samples

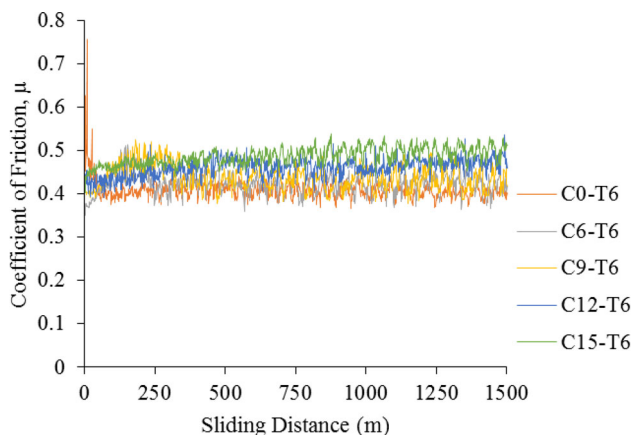


Fig. 10 Friction coefficients of the artificially aged samples

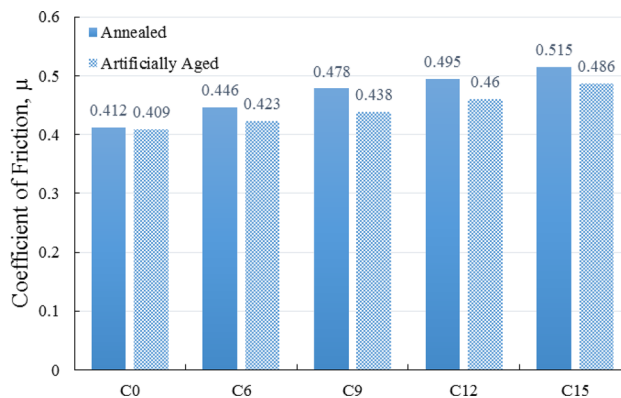
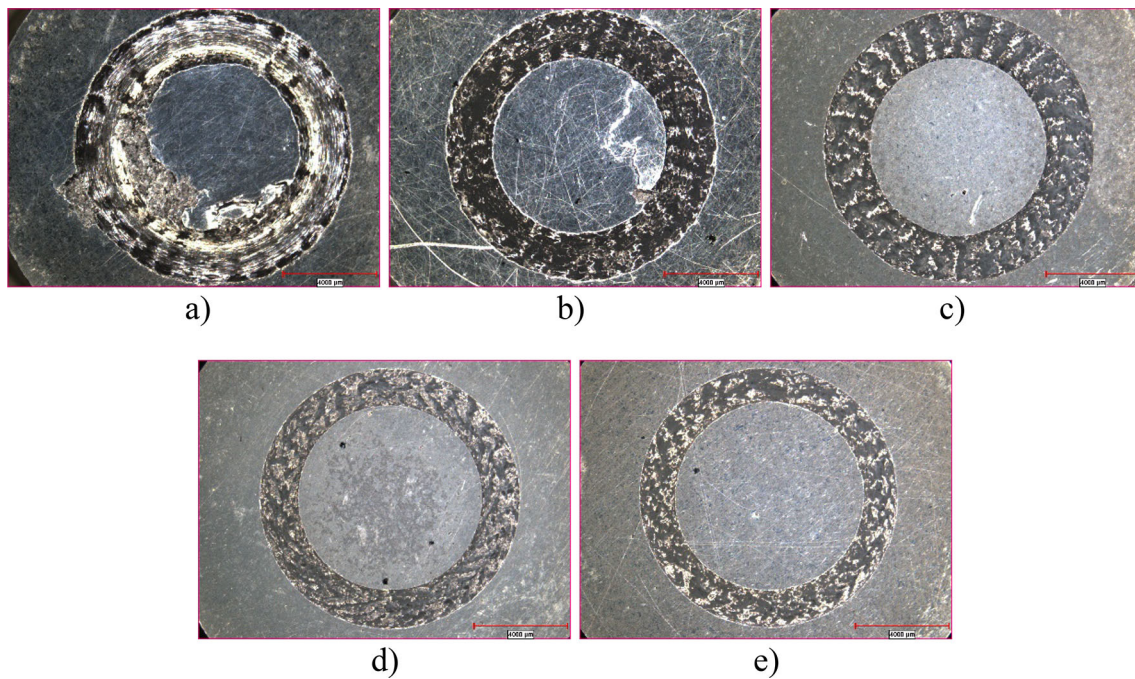


Fig. 11 Average friction coefficients of all samples

53.1, 79.5, 83.6, 96.3 and 117.3 for the C0-O, C6-O, C9-O, C12-O and C15-O, successively [32].

Figures 3 and 4 represent the volumetric wear loss of the investigated nanocomposites with respect to sliding distance. It can be seen apparently that the wear loss is very high at the sliding distance of 250 m. With a further increase in the sliding distance, its increment tends to be slowing down significantly. The wear loss of all materials decreases with an increase in the reinforcement content severely. Meantime, the artificially aged composites possess much lower wear losses compared to the annealed ones with the same amount of hybrid reinforcement throughout the testing. The volume loss is 14.9 and 2.9 mm<sup>3</sup> for the C0-O and C0-T6 after the first 250 m, while it increases to 24.9 and 8.2 mm<sup>3</sup> at 1500 m for the same samples, respectively. On the other hand, the volume loss of the samples C15-O and C15-T6 is only 1.6 and 0.7 mm<sup>3</sup> at 250 m and 4.6 and 3.2 mm<sup>3</sup> at 1500 m, successively. It is thought that this is directly related to the higher hardness/elastic module ratio, ( $H/E_r$ ), reached in the nanocomposites with both the aging and the hybrid reinforcement [32]. The ( $H/E_r$ ) is an important indicator for the evaluation of a material's strength under the plastic deformation caused by an indentation contact [39–43]. It was found to be between 0.0090 and 0.0200 for the annealed materials, whereas it changed in the range of 0.0120 and 0.0207 for the aged counterparts in an increasing manner with the reinforcement ratio [32]. In this study, a direct correlation is recorded between the  $H/E_r$  and the wear resistance of the investigated nanocomposites.

Figures 5 and 6 delineate the VWRs of the nanocomposites in the annealed or peak-aged conditions, successively. Although the slope is very steep at the initial step of the testing which corresponds to 250 m, its steepness decreases sharply with the sliding distance and reinforcement ratio. These figures bring out that the sliding wear up to 250 m is considered to be in the transient state at which the severe wear occurs [44–46]. The transient-state wear exists for both the



**Fig. 12** The surface images of annealed samples after the wear test: **a** C0-O, **b** C6-O, **c** C9-O, **d** C12-O and **e** C15-O

Al–4Cu alloy and the hybrid reinforced aluminum nanocomposites due to the fact that the hard asperities of W–6Co ball remove their soft asperities more easily during the initial metal–metal contact causing more metallic loss as a loose wear debris [44–46]. Hence, the excessive wear loss is available in the transient zone. The steady-state wear behavior develops throughout the sliding distance greater than 250 m. There are basically two kinds of wear regimes in sliding wear of aluminum alloys, namely mild and severe [47, 48]. The material loss during the sliding wear of aluminum alloys is at quite low levels in mild wear due to the formation of tribolayers and lower plastic deformation on contact surface [48]. Mild wear exists at low loads and low sliding speeds while severe wear dominates at higher loads in aluminum alloys [48]. Severe wear, at which extensive surface damage and large amount of material transfer generate between counterface and alloy on contact surface, leads to very high wear rates [48]. The transition level from mild to severe wear in terms of VWR was described for aluminum alloys in an extensive study conducted by Zhang and Alpas [48]. In the present study, it was taken into consideration to specify the wear types for the investigated cases (Fig. 7) [48].

The VWRs decline with an increase in the sliding distance and the hybrid reinforcement ratio for all cases (Figs. 5, 6, 7). In addition, much lower wear rates are reported for the artificially aged nanocomposites. The incorporation of the hybrid reinforcement is appeared to be effective in reduction of the wear rates of the nanocomposites. A similar tendency was

pointed out by some other researchers for the Al 5083/B<sub>4</sub>C<sub>p</sub> and CNT [26] and pure Al/MWCNT + Al<sub>2</sub>O<sub>3p</sub> composites [28]. The span of transient-state region is found to be independent from the reinforcement ratio and the heat treatment. However, its influence on the wear loss decreases substantially with an increase in the amount of reinforcement and the aging. The VWR of the alloys C0-O and C0-T6 reaches about  $5.96 \times 10^{-2}$  and  $1.16 \times 10^{-2} \text{ mm}^3 \text{ m}^{-1}$  in the transient stage (0–250 m), respectively. However, it becomes nearly  $4.80 \times 10^{-3}$  and  $4.50 \times 10^{-3} \text{ mm}^3 \text{ m}^{-1}$  at the 1500 m for them, successively. On the other hand, the lowest VWR, obtained for the C15-T6 at 1500 m, is  $\sim 1.79 \times 10^{-3} \text{ mm}^3 \text{ m}^{-1}$ . Among the annealed samples, only the C12-O and C15-O fall into the mild wear regime under the steady-state circumstance (after 500 m) but all the aged samples lie in the mild wear zone (Fig. 7). It should be remembered that the counter material as in the form of ball was the cemented carbide, WC–6Co with a hardness of  $\sim 1881 \text{ HV}_{0.1}$ . For this reason, the alloy and the annealed nanocomposites were exposed to much higher wear rates because of their relatively lower hardness [32].

Figure 8 presents the wear coefficients of the investigated materials that were computed by Eqs. 2–4 [5, 37, 38]. The artificially aged composites have smaller wear coefficients in comparison with the annealed counterparts. Furthermore, the wear coefficient of the artificial aged nanocomposites reduces with an increase in the reinforcement proportion gradually. The higher hardness of the aged composites combined with the uniform reinforcement dispersion by the mechanical

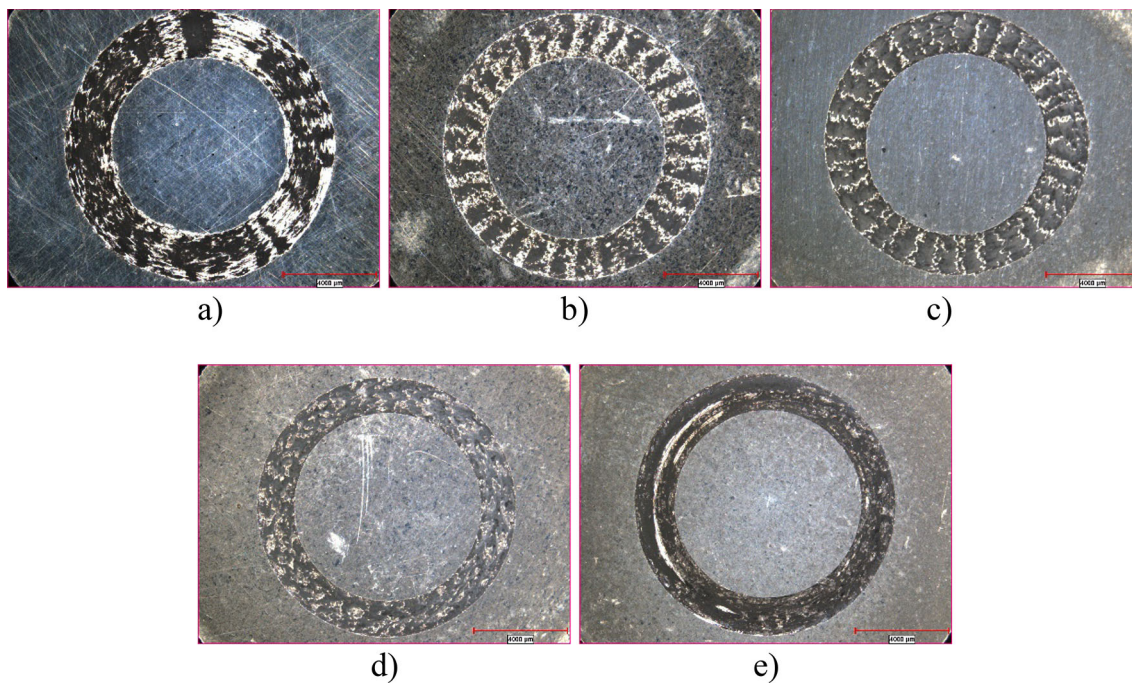


Fig. 13 The surface pictures of the artificially aged samples after the wear test: **a** C0-T6, **b** C6-T6, **c** C9-T6, **d** C12-T6 and **e** C15-T6

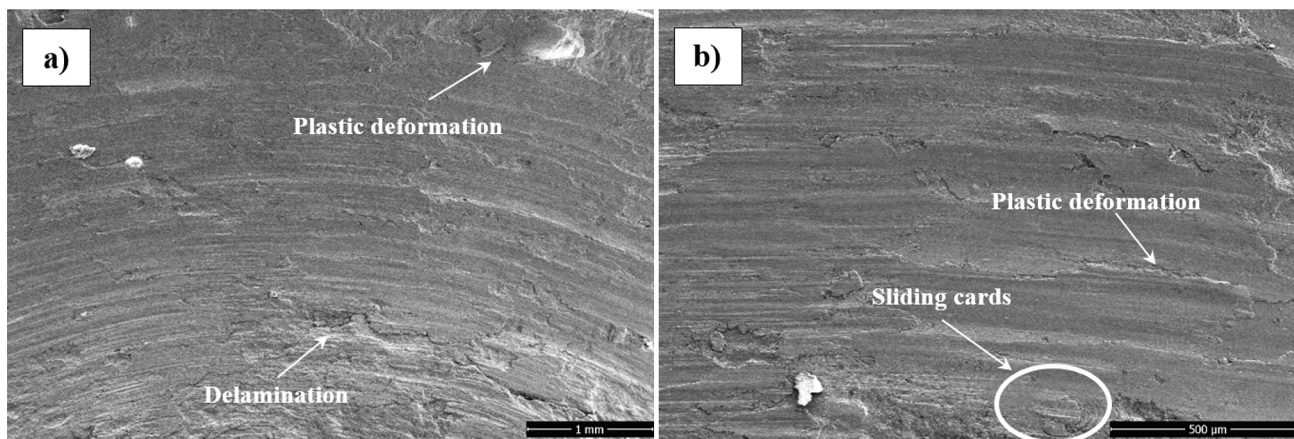
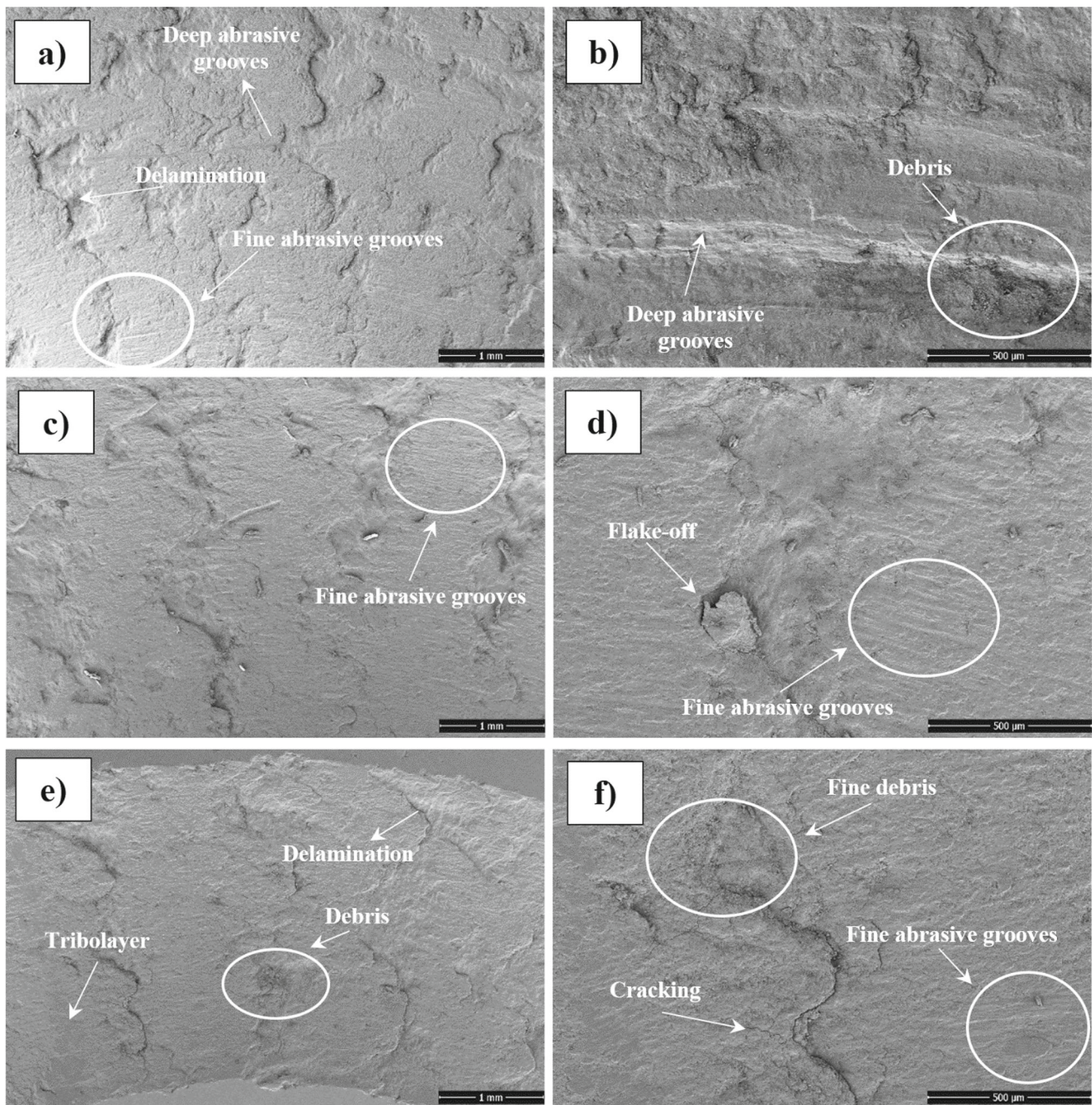


Fig. 14 The typical worn surface of the C0-O after a track of 1500 m

alloying [32] is mainly supposed to be responsible for the lower wear coefficients. The coefficients of friction for the annealed and aged composites versus sliding distance are displayed in Figs. 9 and 10, respectively. Their mean values are also depicted in Fig. 11. It can be apparently seen that the lower friction coefficients are available for the aged nanocomposites. Moreover, increasing the hybrid reinforcement ratio leads to a little bit higher coefficients of friction.

Figures 12 and 13 depict the general view of wear track on the samples created by the ball’s motion under the load of 10 N. The width of traces becomes narrower with increase in the

hybrid reinforcement content since the plastic deformation is restricted seriously when the hardness of the nanocomposite is increased, as expected. Figure 14 illustrates the worn surface of the C0-O after a track length of 1500 m. One can clearly observe that the abrasive wear is dominant in the annealed alloy where the deep grooves were formed by microcutting and microplowing [4, 5] actions of the WC–6Co ball under the applied load. Meantime, an extensive plastic deformation with some sliding cards [49, 50] and some cracks parallel to the sliding direction are also detected. In the C6-O, C9-O and C12-O nanocomposites, the abrasive wear



**Fig. 15** The worn surfaces of C6-O (a, b), C9-O (c, d) and C12-O (e, f)

and delamination, that are mainly responsible for the wear loss, take place together (Fig. 15). The grooves on the worn surfaces of these composites are found to be shallower than those of the C0-O owing to their relatively higher hardness.

Furthermore, the fragmented oxidized layer and powdery debris on their worn surfaces of the C0-O, C6-O, C9-O and C12-O are observed but the oxidized layer does not seem to be operative and efficient for reducing wear loss (Figs. 16,

17). With a further increase in the hybrid reinforcement content, the oxidative wear becomes the primary mechanism. Figure 18 shows the SEM pictures of the worn surface of the sample, C15-O. The delamination and the fracture of oxidized tribolayer on its worn surface are observed extensively. And also, the cracks, being perpendicular to the sliding direction, are detected frequently as well. Moreover, there



**Fig. 16** EDX analysis of some selected points on the C0-O

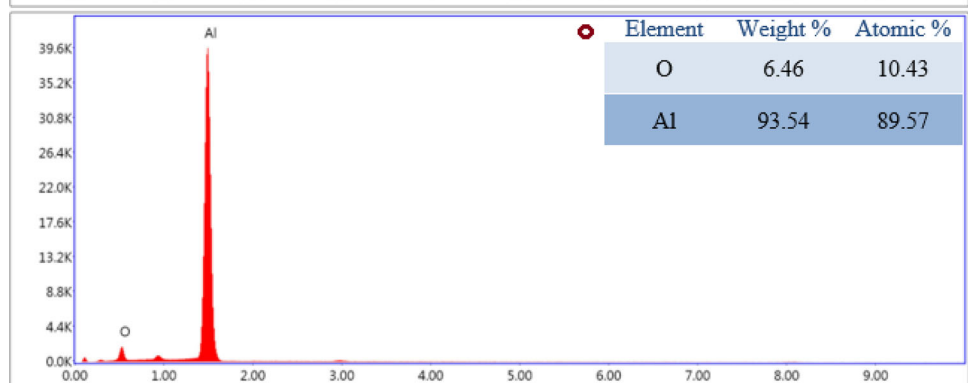
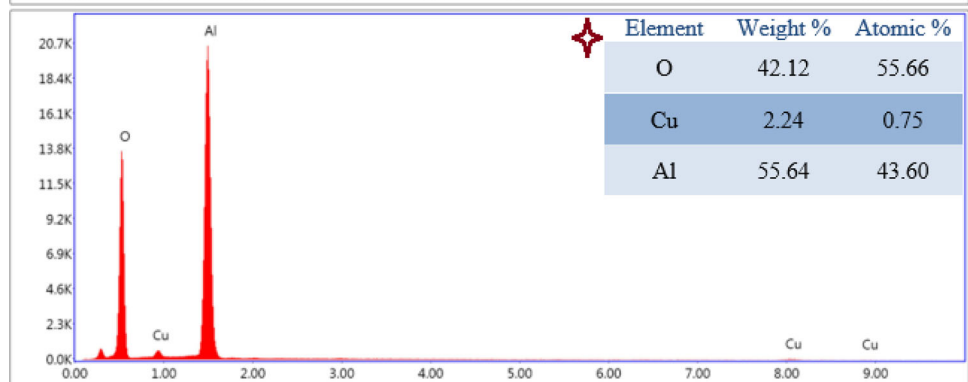
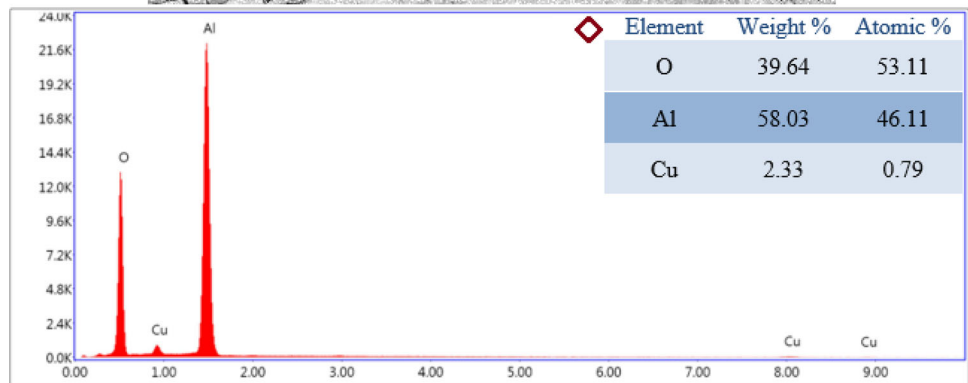
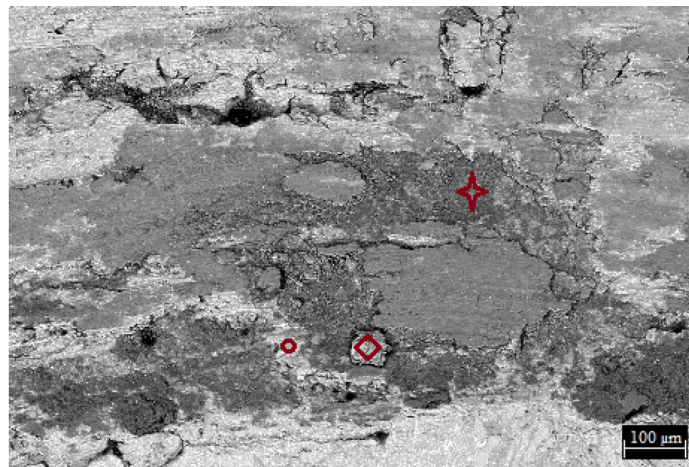
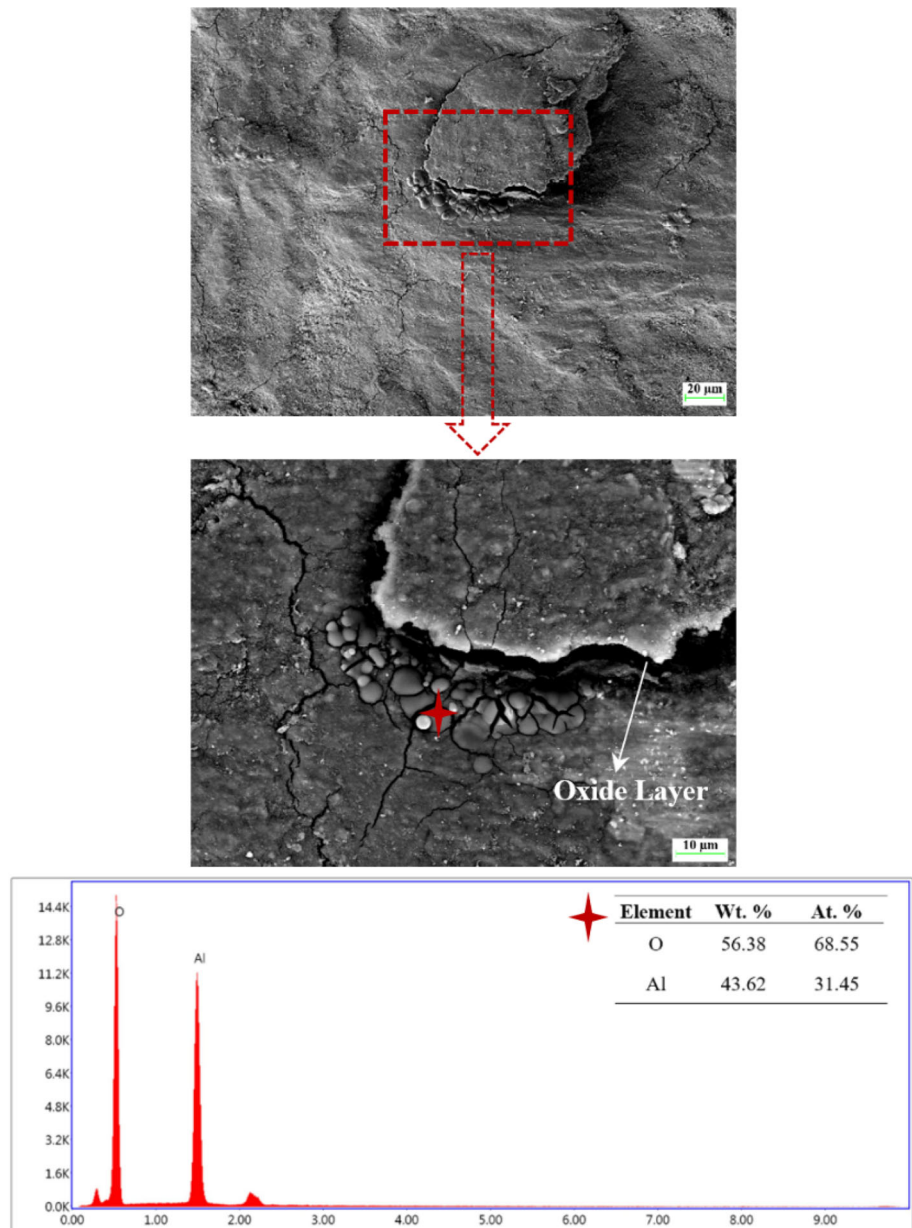


**Fig. 17** EDX analysis on the worn surface of C6-O



are some very fine abrasive lines located on the tribolayers. Figure 19 represents the EDX analyses of some selected points on the worn surface of C15-O at which the very high oxygen levels are detected.

The contact of two solid surfaces under dry sliding induces the normal and tangential forces on the softer surface which cause the formation of plastic deformation zone just below the contact surface [51]. In the plastic deformation zone, the initiation, propagation and coalescence of cracks are observed at a certain depth below the contact surface with continuous sliding [51]. The formation of cracks and voids

is triggered in this zone under the cyclic loading throughout the wear process due to the accumulation of large plastic strains [51, 52]. While the cracks intersect the contact surface, delamination mechanism, which can result in severe wear, takes place by producing wear debris in the form of thin wear plates [51]. The depth of the plastically deformed zone is highly affected by the properties of the worn material as well as the processing variables [51–53]. The dominance of abrasion and delamination mechanisms in the annealed samples (except for C15-O) is attributed to their relatively lower resistance to plastic deformations. The entrapped wear debris between the sliding couple can be oxidized easily due

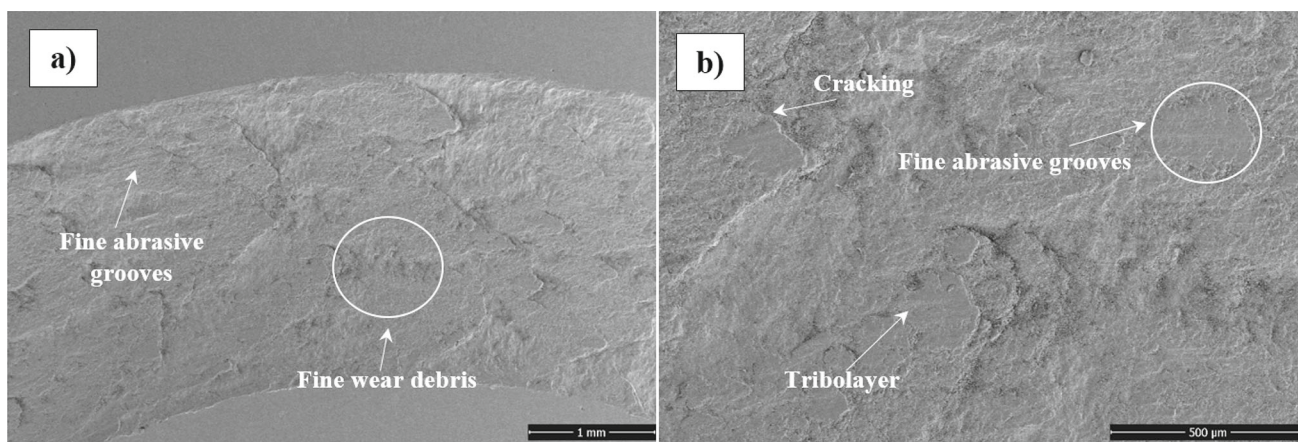


Fig. 18 SEM images of the worn surface of C15-O

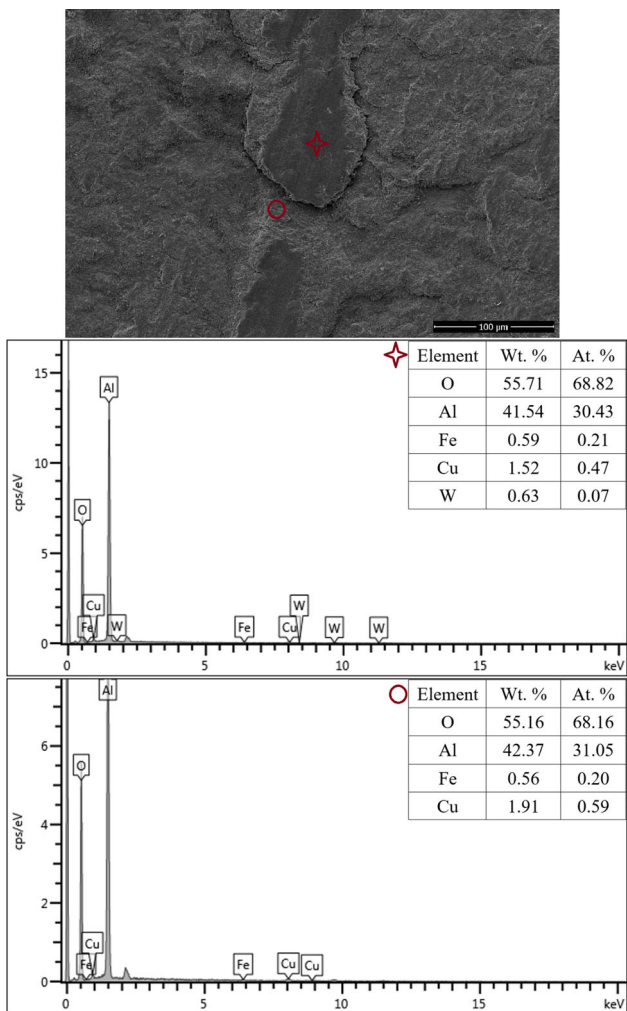
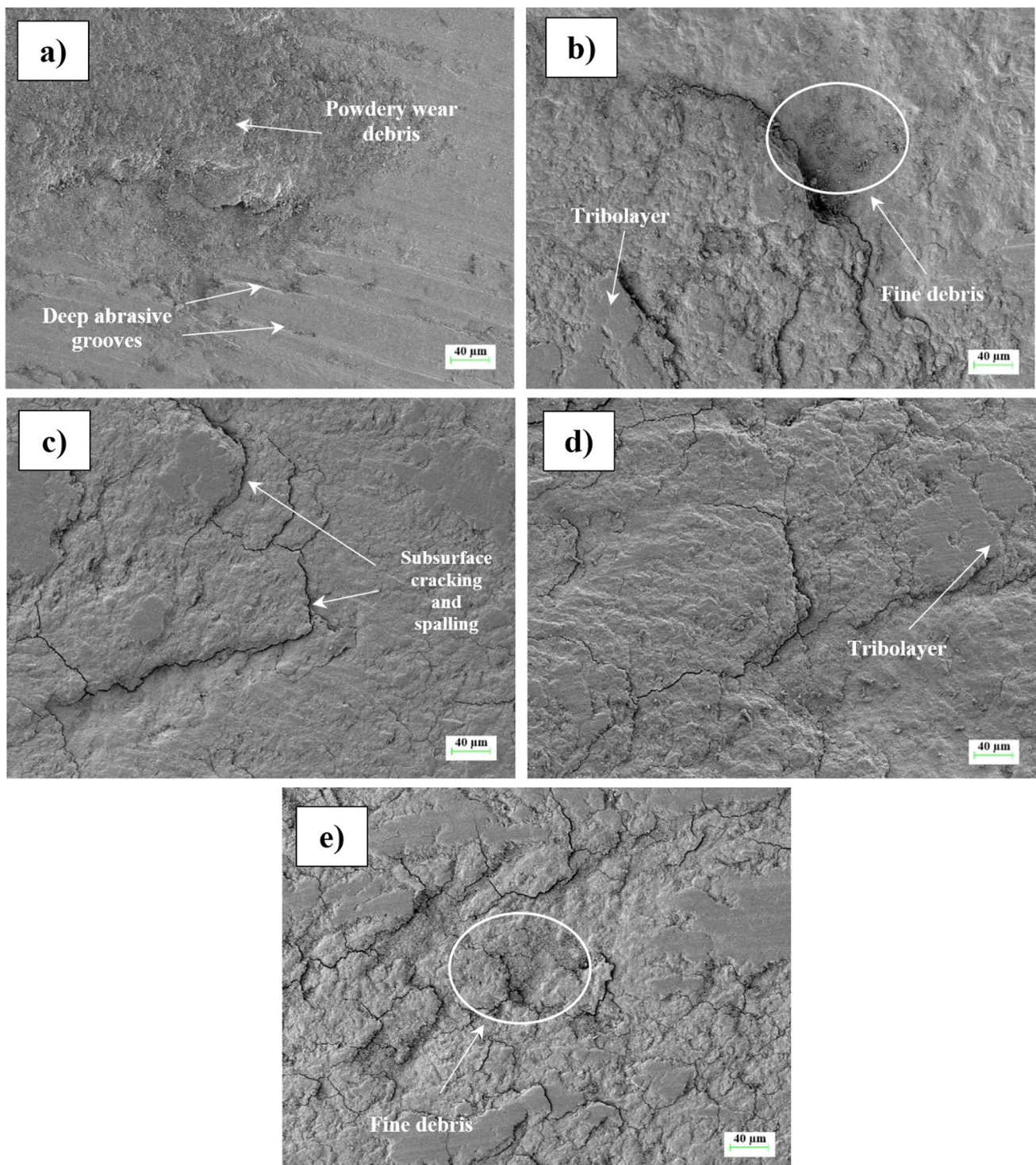


Fig. 19 EDX analysis on the tribolayer formed at the worn surface of C15-O

to the heating by frictional forces [46, 48, 54] and the very high affinity of aluminum to oxygen [33]. In addition to the aluminum oxide, metallic and reinforcement particles (nano- $\text{Al}_2\text{O}_3$  and MWCNT) as well as possible particles (W and Co) detached from the ball take part in the wear debris by the mechanically mixing effect of the WC-6Co ball in the course of sliding. After the mechanically mixed layer, also known as tribolayer or transfer layer, is formed, it is compacted and broken into pieces by the counterface [48, 52, 55–63]. With the continuous sliding, the oxide tribolayer is reformed and again subjected to compaction-fracture-reformation cycles [48, 52, 55–63]. The wear debris is also generated by the detachment or spalling of some fragmented particles of the layer under the loading. The tribolayer serves as a lubricating agent between the nanocomposite and the counterface by reducing the direct contact of the surfaces [48, 52, 55–63]. And also, it prevents the adhesive wear on the nanocomposites at a great extent by forming an insulating layer due to its high hardness [48, 52, 55–63].

The surface photographs of the aged samples after the wear tests are illustrated in Fig. 20. In the C0-T6 sample, the deep grooves are widely detected, that is why the abrasive wear, causing high wear rates, is found to be the dominant wear type as in the case of C0-O. And also, the powdery wear debris is also recorded at some locations of the worn surface of C0-T6. However, the oxidative wear is appeared to be the common wear type for the aged nanocomposites. The oxide tribolayer, as well as the long axial and lateral cracks related to the delamination mechanism on the worn surfaces of aged nanocomposites are seen clearly in Fig. 20. Furthermore, the destruction of tribolayer on the worn surface of the C15-T6 is illustrated in Fig. 21. In the worn surfaces of the nanocomposites, C15-O and C15-T6, the detachment of some particles from the ball is recorded on the tribolayer which means that



**Fig. 20** SEM pictures of the worn surfaces for: **a** C0-T6, **b** C6-T6, **c** C9-T6, **d** C12-T6 and **e** C15-T6

the increment in the reinforcing phases makes the nanocomposite more resistant to abrasion (Figs. 19, 22). The decline in the VWR with increase in the reinforcement amount is closely related to the oxidative wear mechanism as well as the higher  $H/E_r$  levels in the aged nanocomposites. The

aged nanocomposites withstood the abrasive and delamination wear more successfully compared to the annealed ones.

In order to restrict the plastic deformation region and inhibit the abrasion and delamination at a major scale, not only the high strength and hardness levels of the composites

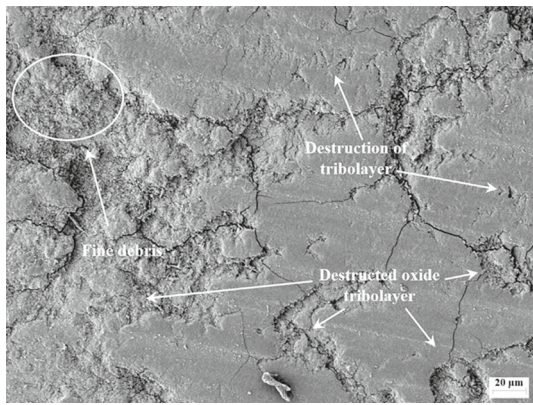
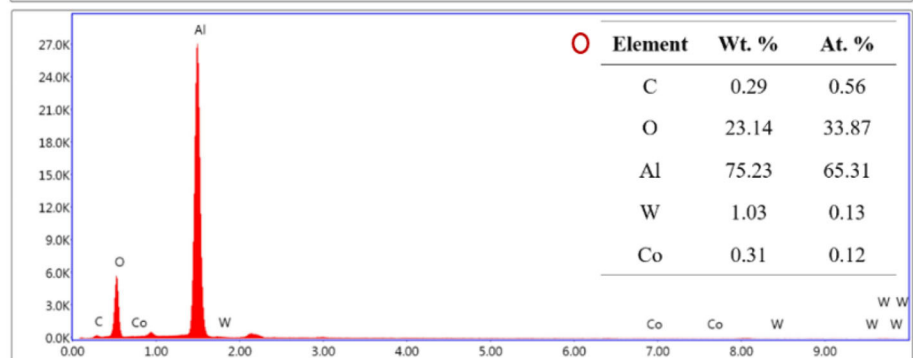
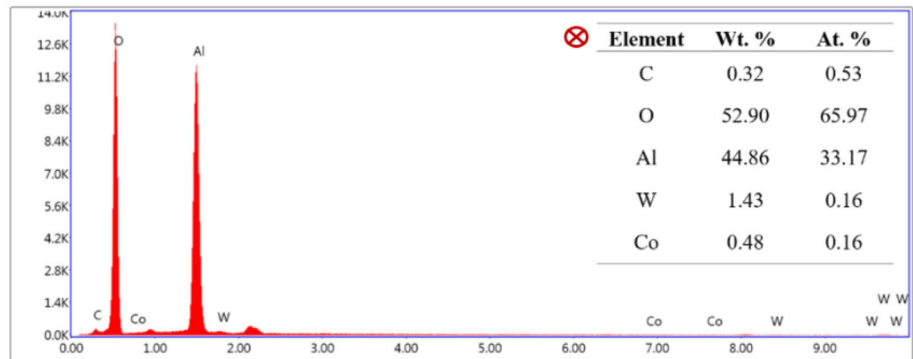
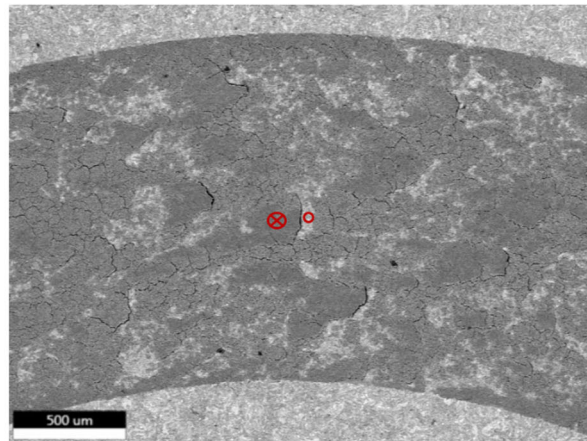


Fig. 21 Destruction of tribolayer on the C15-T6

but also the strong bonding and cohesion between the matrix and the reinforcement are strongly required [26, 61, 64, 65]. On the other hand, the formation of tribolayer helps very much in reducing the severe plastic deformation on the worn surface of the aged nanocomposites. The higher hardness levels of the aged nanocomposites, gained owing to the presence of nanoparticles (alumina and MWCNT) and Al<sub>2</sub>Cu precipitates throughout the matrix [32], play a major role for resisting the plastic deformation induced by the cyclic loading in the course of sliding wear. The homogeneous dispersion of these nanoparticles [32] with smaller interparticle spacing and good bonding with the Al-4Cu matrix are considered to be very effective in preventing the dislocation motion and thereby constricting plastic deformation [61, 64–67]. Moreover, they improve the load carrying capacity

Fig. 22 EDX analysis on the wear track of C15-T6



of such nanocomposites [67]. Previous studies showed that the reduction in the reinforcement size improved the wear resistance of the aluminum composites, remarkably [59, 68]. The reinforcement with larger particle can be pulled out more easily from the matrix and it acts as a third body between the contact surface and the abrasive media which fastens the wear rate [68].

## 4 Conclusions

Increasing the hybrid reinforcement of the nanocomposites and the artificial aging treatment were recorded to be very beneficial and effective for reducing the wear of the Al–Cu nanocomposites. The volume loss was recorded as 14.9 and 2.9 mm<sup>3</sup> for the C0-O and C0-T6 after the first 250 m, while it increased to 24.9 and 8.2 mm<sup>3</sup> at 1500 m for the same samples, respectively. On the other hand, the volume loss of the samples C15-O and C15-T6 was found to be only 1.6 and 0.7 mm<sup>3</sup> at 250 m and 4.6 and 3.2 mm<sup>3</sup> at 1500 m, successively. In addition, the VWRs declined with an increase in the sliding distance and the hybrid reinforcement ratio for all cases, significantly. The VWR at 1500 m became nearly  $4.80 \times 10^{-3}$  and  $4.50 \times 10^{-3}$  mm<sup>3</sup> m<sup>-1</sup> for the alloys C0-O and C0-T6, successively while it decreased to  $\sim 1.79 \times 10^{-3}$  mm<sup>3</sup> m<sup>-1</sup> for the C15-T6.

The average wear coefficient changed between 0.409 and 0.515 depending on the reinforcement content and heat treatment of the nanocomposites. The artificially aged composites had smaller wear coefficients in comparison with the annealed counterparts. In the annealed samples (except for C15-O), the main wear types were determined to be abrasive wear and delamination while the oxidative wear was dominant in the aged nanocomposites. The increase in the hybrid reinforcement ratio in these composites enhanced the resistance of the alloy against the plastic deformation, abrasion and delamination wear seriously. Moreover, the T6 treatment application was appeared to be very crucial for both the conversion of the severe wear to the mild wear and the reduction in the wear loss during the transient state in the investigated nanocomposites.

**Funding** Open access funding provided by the Scientific and Technological Research Council of Türkiye (TÜBİTAK).

## Declarations

**Conflict of interest** The authors declare that they have no conflict interest.

**Open Access** This article is licensed under a Creative Commons Attribution 4.0 International License, which permits use, sharing, adaptation, distribution and reproduction in any medium or format, as long as you

give appropriate credit to the original author(s) and the source, provide a link to the Creative Commons licence, and indicate if changes were made. The images or other third party material in this article are included in the article's Creative Commons licence, unless indicated otherwise in a credit line to the material. If material is not included in the article's Creative Commons licence and your intended use is not permitted by statutory regulation or exceeds the permitted use, you will need to obtain permission directly from the copyright holder. To view a copy of this licence, visit <http://creativecommons.org/licenses/by/4.0/>.

## References

- Ceschini, L.; Dahle, A.; Gupta, M.; Jarfors, A.E.W.; Jayalakshmi, S.; Morri, A.; Rotundo, F.; Toschi, S.; Singh, R.A.: Aluminum and Magnesium Metal Matrix Nanocomposites. Springer, Singapore (2017)
- Kim, C.; Cho, K.; Manjili, M.H.; Nezafati, M.: Mechanical Performance of particulate-reinforced Al metal-matrix composites (MMCs) and Al metal-matrix nano-composites (MMNCs). *J. Mater. Sci.* **52**, 13319–13349 (2017). <https://doi.org/10.1007/s10853-017-1378-x>
- Ashby, M.F.; Ferreira, P.J.; Schodek, D.L.: Nanomaterials, Nanotechnologies and Design. Butterworth-Heinemann (2009)
- Stachowiak, G.W.; Batchelor, A.W.: Engineering Tribology. Elsevier Butterworth-Heinemann (2014)
- Hutchings, I.; Shipway, P.: Tribology, Friction and Wear of Engineering Materials. Elsevier Butterworth-Heinemann (2017)
- Stein, J.; Lenczowski, B.; Anglaret, E.; Fréty, N.: Influence of the concentration and nature of carbon nanotubes on the mechanical properties of AA5083 aluminium alloy matrix composites. *Carbon* **77**, 44–52 (2014). <https://doi.org/10.1016/j.carbon.2014.05.001>
- Kallip, K.; Leparoux, M.; Alogab, K.A.; Clerc, S.; Deguilhem, G.; Arroyo, Y.; Kwon, H.: Investigation of different carbon nanotube reinforcements for fabricating bulk AlMg5 matrix nanocomposites. *J. Alloys Compd.* **646**, 710–718 (2015). <https://doi.org/10.1016/j.jallcom.2015.06.169>
- Deng, C.F.; Wang, D.Z.; Zhang, X.X.; Li, A.B.: Processing and properties of carbon nanotubes reinforced aluminum composites. *Mater. Sci. Eng. A* **444**, 138–145 (2007). <https://doi.org/10.1016/j.msea.2006.08.057>
- Esawi, A.M.K.; Morsi, K.; Sayed, A.; Taher, M.; Lanka, S.: Effect of carbon Nanotube (CNT) content on the mechanical properties of CNT-reinforced aluminium composites. *Compos. Sci. Technol.* **70**, 2237–2241 (2010). <https://doi.org/10.1016/j.compscitech.2010.05.004>
- Asgharzadeh, H.; Kim, H.S.; Simchi, A.: Microstructure, strengthening mechanisms and hot deformation behavior of an oxide-dispersion strengthened UFG Al6063 alloy. *Mater. Charact.* **75**, 108–114 (2013). <https://doi.org/10.1016/j.matchar.2012.10.007>
- Babu, N.K.; Kallip, K.; Leparoux, M.; AlOgab, K.A.; Maeder, X.; Dasilva, Y.A.R.: Influence of microstructure and strengthening mechanism of AlMg5–Al<sub>2</sub>O<sub>3</sub> nanocomposites prepared via spark plasma sintering. *Mater. Des.* **95**, 534–544 (2016). <https://doi.org/10.1016/j.matdes.2016.01.138>
- Dash, K.; Chaira, D.; Ray, B.C.: Synthesis and characterization of aluminium–alumina micro- and nano-composites by spark plasma sintering. *Mater. Res. Bull.* **48**, 2535–2542 (2013). <https://doi.org/10.1016/j.materresbull.2013.03.014>
- Kang, Y.C.; Chan, S.L.I.: Tensile properties of nanometric Al<sub>2</sub>O<sub>3</sub> particulate-reinforced aluminum matrix composites. *Mater. Chem. Phys.* **85**, 438–443 (2004). <https://doi.org/10.1016/j.matchemphys.2004.02.002>
- Rahman, M.A.; Sirajudeen, N.; Patnaik, S.: Effect of different heat treatments and varying volume fraction of nano-Al<sub>2</sub>O<sub>3</sub> particles on

- the hardness and wear resistance of Al 7150 alloy matrix composite synthesized by hot uniaxial compaction technique. *Mater. Res. Express* **6**, 086515 (2019). <https://doi.org/10.1088/2053-1591/ab1a1c>
15. Sadeghi, B.; Shamanian, M.; Ashrafzadeh, F.; Cavaliere, P.; Rizzo, A.: Wear behavior of Al-based nanocomposites reinforced with bimodal micro- and nano-sized Al<sub>2</sub>O<sub>3</sub> particles produced by spark plasma sintering. *Mater. Perform. Charact.* **7**, 327–350 (2018). <https://doi.org/10.1520/MPC20180039>
  16. Shrivastava, V.; Dubey, S.; Gupta, G.K.; Singh, I.B.: Influence of alpha nanoalumina reinforcement content on the microstructure, mechanical and corrosion properties of Al6061-Al<sub>2</sub>O<sub>3</sub> composite. *J. Mater. Eng. Perform.* **26**, 4424–4433 (2017). <https://doi.org/10.1007/s11665-017-2893-2>
  17. Abdullahi, U.; Maleque, M.A.; Nirmal, U.: Wear mechanisms map of CNT-Al nano-composite. *Procedia Eng.* **68**, 736–742 (2013). <https://doi.org/10.1016/j.proeng.2013.12.247>
  18. Omid, M.; Khodabandeh, A.; Nategh, S.; Khakbiz, M.: Microstructural and tribological properties of nanostructured Al6061-CNT produced by mechanical milling and extrusion. *Adv. Powder Technol.* **29**, 543–554 (2018). <https://doi.org/10.1016/j.apt.2017.12.026>
  19. Wang, L.Z.; Liu, Y.; Wu, J.J.; Zhang, X.: Mechanical properties and friction behaviors of CNT/AlSi10Mg composites produced by spark plasma sintering. *Int. J. Miner. Metall. Mater.* **24**, 584–593 (2017). <https://doi.org/10.1007/s12613-017-1440-3>
  20. Shivaramu, H.T.; Umashankar, K.S.: Dry Sliding wear behaviour of multi walled carbon nanotubes reinforced aluminium composites produced by powder metallurgy technique. *Mater. Res. Express.* **6**, 1150d7 (2019). <https://doi.org/10.1088/2053-1591/ab501f>
  21. Kwon, H.; Cho, S.; Leparoux, M.; Kawasaki, A.: Dual-nanoparticulate-reinforced aluminum matrix composite materials. *Nanotechnology* **23**, 225704 (2012). <https://doi.org/10.1088/0957-4484/23/22/225704>
  22. Kwon, H.; Leparoux, M.; Kawasaki, A.: Functionally graded dual-nanoparticulate-reinforced aluminium matrix bulk materials fabricated by spark plasma sintering. *J. Mater. Sci. Technol.* **30**, 736–742 (2014). <https://doi.org/10.1016/j.jmst.2014.03.003>
  23. Kwon, H.; Saarna, M.; Yoon, S.; Weidenkaff, A.; Leparoux, M.: Effect of milling time on dual-nanoparticulate-reinforced aluminum alloy matrix composite materials. *Mater. Sci. Eng. A* **590**, 338–345 (2014). <https://doi.org/10.1016/j.msea.2013.10.046>
  24. Toozandehjani, M.; Matori, K.A.; Ostovan, F.; Jamaludin, K.R.; Amrin, A.; Shafiei, E.: The effect of the addition of CNTs on the microstructure, densification and mechanical behavior in Al-CNT-Al<sub>2</sub>O<sub>3</sub> hybrid nanocomposites. *J. Miner. Met. Mater. Soc. (JOM)* **72**, 2283–2294 (2020). <https://doi.org/10.1007/s11837-020-04132-5>
  25. Kim, W.J.; Yu, Y.J.: The effect of the addition of multiwalled carbon nanotubes on the uniform distribution of TiC nanoparticles in aluminum nanocomposites. *Scr. Mater.* **72–73**, 25–28 (2014). <https://doi.org/10.1016/j.scriptamat.2013.10.008>
  26. Alizadeh, A.; Abdollahi, A.; Biukani, H.: Creep behavior and wear resistance of Al 5083 based hybrid composites reinforced with carbon nanotubes (CNTs) and boron carbide (B<sub>4</sub>C). *J. Alloys Compd.* **650**, 783–793 (2015). <https://doi.org/10.1016/j.jallcom.2015.07.214>
  27. Zayed, A.S.; Kamel, B.M.; Osman, T.A.; Elkady, O.A.; Ali, S.: Experimental study of tribological and mechanical properties of aluminum matrix reinforced by Al<sub>2</sub>O<sub>3</sub>/CNTs. *Fuller. Nanotub. Car. N.* **27**, 538–544 (2019). <https://doi.org/10.1080/1536383X.2019.1612882>
  28. Ostovan, F.; Amanollah, S.; Toozandehjani, M.; Shafiei, E.: Fabrication of Al5083 surface hybrid nanocomposite reinforced by CNTs and Al<sub>2</sub>O<sub>3</sub> nanoparticles using friction stir processing. *J. Compos. Mater.* **54**, 1107–1117 (2020). <https://doi.org/10.1177/0021998319874849>
  29. Prakash, C.; Singh, S.; Sharma, S.; Garg, H.; Singh, J.; Kumar, H.; Singh, G.: Fabrication of aluminium carbon nano tube silicon carbide particles based hybrid nano-composite by spark plasma sintering. *Mater. Today Proc.* **21**, 1637–1642 (2020). <https://doi.org/10.1016/j.matpr.2019.11.273>
  30. Zhang, X.; Li, S.; Pan, D.; Pan, B.; Kondoh, K.: Microstructure and synergistic-strengthening efficiency of CNTs-SiCp dual-nano reinforcements in aluminum matrix composites. *Compos. Part A Appl. Sci. Manuf.* **105**, 87–96 (2018). <https://doi.org/10.1016/j.compositesa.2017.11.013>
  31. Saba, F.; Sajjadi, S.A.; Haddad-Sabzevar, M.; Zhang, F.: Exploring the reinforcing effect of TiC and CNT in dual-reinforced Al-matrix composites. *Diam. Relat. Mater.* **89**, 180–189 (2018). <https://doi.org/10.1016/j.diamond.2018.09.007>
  32. Özer, E.; Ayvaz, M.; Übeyli, M.; Sarpkaya, İ.: Properties of aluminum nano composites bearing alumina particles and multi-wall carbon nanotubes manufactured by mechanical alloying and microwave sintering. *Met. Mater. Int.* **29**, 402–419 (2023). <https://doi.org/10.1007/s12540-022-01238-0>
  33. Davis, J.R.: *ASM Specialty Handbook, Aluminum and Aluminum Alloys*. ASM International (1993)
  34. ASTM E384-17: Standard Test Method for Microindentation Hardness of Materials. ASTM International, West Conshohocken (2017)
  35. ASTM G99-17 Group: Standard Test Method for Wear Testing with a Pin-On-Disk Apparatus. ASTM International, West Conshohocken (2017)
  36. Totten, G.E.: *ASM Handbook, Volume 18: Friction, Lubrication, and Wear Technology*. ASM International (2017)
  37. Archard, J.F.: Contact and rubbing of flat surfaces. *J. Appl. Phys.* **24**, 981–988 (1953). <https://doi.org/10.1063/1.1721448>
  38. Yang, L.J.: Wear coefficient equation for aluminium-based matrix composites against steel disc. *Wear* **255**, 579–592 (2003). [https://doi.org/10.1016/S0043-1648\(03\)00191-1](https://doi.org/10.1016/S0043-1648(03)00191-1)
  39. Cheng, Y.-T.; Cheng, C.-M.: Relationships between hardness, elastic modulus and the work of indentation. *Appl. Phys. Lett.* **73**, 614–616 (1998). <https://doi.org/10.1063/1.121873>
  40. Cheng, Y.-T.; Cheng, C.-M.: Scaling, Dimensional Analysis and indentation measurements. *Mater. Sci. Eng. R. Rep.* **44**, 91–149 (2004). <https://doi.org/10.1016/j.mser.2004.05.001>
  41. Leyland, A.; Matthews, A.: On the Significance of the H/E ratio in wear control: a nanocomposite coating approach to optimized tribological behaviour. *Wear* **246**, 1–11 (2000). [https://doi.org/10.1016/S0043-1648\(00\)00488-9](https://doi.org/10.1016/S0043-1648(00)00488-9)
  42. Bhoi, N.K.; Singh, H.; Pratap, S.: Synthesis and characterization of zinc oxide reinforced aluminum metal matrix composite produced by microwave sintering. *J. Compos. Mater.* **54**, 3625–3636 (2020). <https://doi.org/10.1177/0021998320918646>
  43. Beake, B.D.; Harris, A.J.; Liskiewicz, T.W.: Advanced nanomechanical test techniques. In: Ranganathan, N. (Ed.) *Materials Characterization: Modern Methods and Applications*, pp. 1–89. CRC Press, Boca Raton (2016)
  44. Singh, R.; Shadab, M.; Dash, A.; Rai, R.N.: Characterization of dry sliding wear mechanisms of AA5083/B<sub>4</sub>C metal matrix composite. *J. Braz. Soc. Mech. Sci. Eng.* **41**, 98 (2019). <https://doi.org/10.1007/s40430-019-1593-2>
  45. Zhang, Z.F.; Zhang, L.C.; Mai, Y.W.: Wear of ceramic particle-reinforced metal-matrix composites: part I wear mechanisms. *J. Mater. Sci.* **30**, 1961–1966 (1995). <https://doi.org/10.1007/BF00353018>
  46. Razavizadeh, K.; Eyre, T.S.: Oxidative wear of aluminium alloys. *Wear* **79**, 325–333 (1982). [https://doi.org/10.1016/0043-1648\(82\)90322-2](https://doi.org/10.1016/0043-1648(82)90322-2)



47. Archard, J.F.; Hirst, W.: The wear of metals under unlubricated conditions. *Proc. R. Soc. A: Math. Phys. Eng. Sci.* **236**, 397–410 (1956). <https://doi.org/10.1098/rspa.1956.0144>
48. Zhang, J.; Alpas, A.T.: Transition between mild and severe wear in aluminum alloys. *Acta Mater.* **45**, 513–528 (1997). [https://doi.org/10.1016/S1359-6454\(96\)00191-7](https://doi.org/10.1016/S1359-6454(96)00191-7)
49. Berthier, Y.; Vincent, L.; Godet, M.: Fretting fatigue and fretting wear. *Tribol. Int.* **22**, 235–242 (1989). [https://doi.org/10.1016/0301-679X\(89\)90081-9](https://doi.org/10.1016/0301-679X(89)90081-9)
50. Godet, M.; Berthier, Y.: Continuity and dry friction: an osborne reynolds approach. In: Dowson, D.; Taylor, C.M.; Godet, M.; Berthe, D. (Eds.) *Fluid Film Lubrication—Osborne Reynolds Centenary*, pp. 653–661. Elsevier, Amsterdam (1987)
51. Suh, N.P.: An overview of the delamination theory of wear. *Wear* **44**, 1–16 (1977). [https://doi.org/10.1016/0043-1648\(77\)90081-3](https://doi.org/10.1016/0043-1648(77)90081-3)
52. Rice, S.L.; Nowotny, H.; Wayne, S.F.: Characteristics of metallic subsurface zones in sliding and impact wear. *Wear* **74**, 131–142 (1981). [https://doi.org/10.1016/0043-1648\(81\)90199-X](https://doi.org/10.1016/0043-1648(81)90199-X)
53. Deus, R.L.; Subramanian, C.; Yellup, J.M.: Dry sliding wear of aluminium composites—a review. *Compos. Sci. Technol.* **57**, 415–435 (1997). [https://doi.org/10.1016/S0266-3538\(96\)00167-4](https://doi.org/10.1016/S0266-3538(96)00167-4)
54. Zhang, J.; Alpas, A.T.: Wear regimes and transitions in Al<sub>2</sub>O<sub>3</sub> particulate-reinforced aluminum alloys. *Mater. Sci. Eng. A* **161**, 273–284 (1993). [https://doi.org/10.1016/0921-5093\(93\)90522-G](https://doi.org/10.1016/0921-5093(93)90522-G)
55. Iwabuchi, A.; Kubosawa, H.; Hori, K.: The dependence of the transition from severe to mild wear on load and surface roughness when the oxide particles are supplied before sliding. *Wear* **139**, 319–333 (1990). [https://doi.org/10.1016/0043-1648\(90\)90054-E](https://doi.org/10.1016/0043-1648(90)90054-E)
56. Iwabuchi, A.; Hori, K.; Kubosawa, H.: The effect of oxide particles supplied at the interface before sliding on the severe-mild wear transition. *Wear* **128**, 123–137 (1988). [https://doi.org/10.1016/0043-1648\(88\)90179-2](https://doi.org/10.1016/0043-1648(88)90179-2)
57. Radhika, N.; Subramanian, R.: Effect of reinforcement on wear behaviour of aluminium hybrid composites. *Tribol. Mater. Surf. Interfaces* **7**, 36–41 (2013). <https://doi.org/10.1179/1751584X13Y.0000000025>
58. Jiang, J.; Stott, F.H.; Stack, M.M.: A mathematical model for sliding wear of metals at elevated temperatures. *Wear* **181–183**, 20–31 (1995). [https://doi.org/10.1016/0043-1648\(95\)90004-7](https://doi.org/10.1016/0043-1648(95)90004-7)
59. Sirajudeen, N.; Abdur Rahman, M.; Haque, S.; Karunanithi, R.; Patnaik, S.: Influence of aging & varying weight fraction of Al<sub>2</sub>O<sub>3</sub> particles on the mechanical behaviour & volumetric wear rate of Al 7075 alloy composite produced by liquid metallurgy route. *Mater. Res. Express.* **6**, 086597 (2019). <https://doi.org/10.1088/2053-1591/ab20b8>
60. Subramanian, C.: Wear Properties of Aluminium-Based Alloys. In: Dong, H. (Ed.) *Surface Engineering of Light Alloys: Aluminium, Magnesium and Titanium Alloys*, pp. 40–57. Woodhead Publishing Limited, UK (2010)
61. Shinde, D.M.; Sahoo, P.; Davim, J.P.: Tribological characterization of particulate-reinforced aluminum metal matrix nanocomposites: a review. *Adv. Compos. Lett.* **29**, 1–28 (2020). <https://doi.org/10.1177/2633366X20921403>
62. Li, X.Y.; Tandon, K.N.: Microstructural Characterization of mechanically mixed layer and wear debris in sliding wear of an Al alloy and an Al based composite. *Wear* **245**, 148–161 (2000). [https://doi.org/10.1016/S0043-1648\(00\)00475-0](https://doi.org/10.1016/S0043-1648(00)00475-0)
63. Riahi, A.R.; Alpas, A.T.: The role of tribo-layers on the sliding wear behavior of graphitic aluminum matrix composites. *Wear* **251**, 1396–1407 (2001). [https://doi.org/10.1016/S0043-1648\(01\)00796-7](https://doi.org/10.1016/S0043-1648(01)00796-7)
64. Singh, M.; Bhandari, D.; Goyal, K.: Wear characteristics of aluminium matrix nanocomposites (AMNCs)—a review. *IOP Conf. Ser. Mater. Sci. Eng.* **1033**, 012010 (2021). <https://doi.org/10.1088/1757-899X/1033/1/012010>
65. Moazami-Goudarzi, M.; Akhlaghi, F.: Wear behavior of Al 5252 alloy reinforced with micrometric and nanometric SiC particles. *Tribol. Int.* **102**, 28–37 (2016). <https://doi.org/10.1016/j.triboint.2016.05.013>
66. Hosseini, N.; Karimzadeh, F.; Abbasi, M.H.; Enayati, M.H.: Tribological properties of Al6061–Al<sub>2</sub>O<sub>3</sub> nanocomposite prepared by milling and hot pressing. *Mater. Des.* **31**, 4777–4785 (2010). <https://doi.org/10.1016/j.matdes.2010.05.001>
67. Mercado-Lemus, V.H.; Gomez-Esparza, C.D.; Díaz-Guillén, J.C.; Mayén-Chaires, J.; Gallegos-Melgar, A.; Arcos-Gutierrez, H.; Hernández-Hernández, M.; Garduño, I.E.; Betancourt-Cantera, J.A.; Perez-Bustamante, R.: Wear dry behavior of the Al–6061–Al<sub>2</sub>O<sub>3</sub> composite synthesized by mechanical alloying. *Metals* **11**, 1652 (2021). <https://doi.org/10.3390/met11101652>
68. Nieto, A.; Yang, H.; Jiang, L.; Schoenung, J.M.: Reinforcement size effects on the abrasive wear of boron carbide reinforced aluminum composites. *Wear* **390–391**, 228–235 (2017). <https://doi.org/10.1016/j.wear.2017.08.002>

